# Synthesis of Gamma Irradiated Cobalt Oxide Nanoparticles for Visible Light-Induced Photocatalytic Degradation of Methylene Blue Dye

Md. Serajum Manir[1], Md. Rabiul Islam[1], Md. Al Mamun[2], Md. Motinur Rahman[3], Md. Firoz Mortuza[4] and Abu Kashem Md. Moshiul Alam[1*]

[1]*Institute of Radiation and Polymer Technology, Atomic Energy Research Establishment (AERE), Bangladesh Atomic Energy Commission (BAEC), Dhaka, Bangladesh*
[2]*Materials Science Division, Atomic Energy Center, Dhaka (AECD), BAEC, Dhaka, Bangladesh*
[3]*Nuclear Electronics Division, Institute of Electronics (IE), AERE, BAEC, Dhaka, Bangladesh*
[4]*Gamma Source Division, Institute of Food and Radiation Biology (IFRB), AERE, BAEC, Dhaka, Bangladesh*

**Abstract**

This research focuses on synthesizing and characterizing cobalt oxide ($Co_3O_4$) nanoparticles using an ionizing radiation technique. The precursor cobalt (III) hydroxide, $Co(OH)_3$ was chemically synthesized from cobalt (II) nitrate hexahydrate, $[Co(NO_3)_2 \cdot 6H_2O]$ as a solution precipitation technique in an alkali medium. The $Co(OH)_3$ precursor was then exposed to a $^{60}Co$ gamma radiation source at a dose of 30 kGy with a dose rate of 10 kGy/hr to obtain $Co_3O_4$ nanoparticles. The synthesized $Co_3O_4$ nanoparticles were subjected to various characterization techniques. Fourier-Transform Infrared (FT-IR) spectroscopic analysis of raw $Co(NO_3)_2 \cdot 6H_2O$, $Co(OH)_3$ precursor, and $Co_3O_4$ nanoparticles revealed distinctive absorption peaks for the $Co_3O_4$ nanoparticles. X-ray diffraction analysis exhibited different characteristic diffraction angles (2θ) values, lattice spacing, and crystal size for the $Co_3O_4$ nanoparticles. SEM images of raw $Co(NO_3)_2 \cdot 6H_2O$, $Co(OH)_3$ precursor, and $Co_3O_4$ nanoparticles displayed distinguishable surface morphologies. Additionally, the thermogravimetric analysis provided insight into the decomposition behaviour of the $Co(OH)_3$ precursor. The characterization data indicated that the ionizing radiation-synthesized $Co_3O_4$ nanoparticles possessed similar properties to those synthesized using conventional methods. Furthermore, the ionizing radiation-synthesized $Co_3O_4$ nanoparticles demonstrated an efficient photo-catalytic effect in the degradation of methylene blue (MB) dye. Therefore, this study shows the successful synthesis and characterization of $Co_3O_4$ nanoparticles using an ionizing radiation technique, highlighting their potential application in photo-catalysis for the degradation of MB dye.

**Keywords:** Ionizing Radiation, Solution Precipitation, Nanoparticles, Photocatalysis, Dye Degradation.

## Introduction

Nowadays, environmental pollution has far-reaching adverse consequences on the lives of living beings. The degradation of organic pollutants, which have a deleterious effect on the health of humankind, has quickly become the center point of research efforts in today's scientific world. Pollutants emitted from various sources pose a severe ecological problem as the biodegradation of these pollutants is often very slow, and

*Corresponding author e-mail: akmmalam@baec.gov.bd

conventional treatments are mostly ineffective and not environmentally compatible. In this regard, the application of photocatalysis, especially photocatalysis using inorganic nanoparticles or nanocomposites system, appears to be the most appealing mean than the more conventional chemical oxidation methods for the decomposition of toxic compounds into non-hazardous products (Chatterjee and Dasgupta, 2005). In catalysis, radiation-induced effects can be controlled to catalyze chemical reactions with exceptional precision and efficiency. Due to their high surface area-to-volume ratio, nanoparticles can be surface-modified by radiation to optimize their catalytic activity, enabling novel and efficient chemical transformations (Song *et al.*, 2022).

In the field of nanoelectronics, radiation plays a significant role in advancing the capabilities of nanoscale devices. By leveraging radiation effects, researchers can manipulate and control nanomaterials' electrical and optical properties, leading to the development of faster, smaller, and more efficient electronic components. Additionally, radiation is employed in magnetic applications, offering opportunities for advancements in areas such as separations, mechanic-chemical conversion, and molecular computing. Nanoparticles can be engineered to exhibit unique magnetic properties, enabling efficient separation of substances, precise control over mechanical movements at the nanoscale, and the potential for molecular-level computing and data storage.

Overall, the combination of radiation effects and nanomaterials has unlocked immense potential for innovation and progress in diverse fields. As the field of nanotechnology continues to evolve, the integration of radiation-based methods is expected to play a pivotal role in pushing the boundaries of what is achievable, facilitating breakthroughs in medicine, energy, materials science, and beyond (Andrzej *et al.*, 2005; Chmielewski *et al.*, 2007).

Traditional methods used to synthesize these nanoparticles include hydrothermal synthesis, sol-gel technique, laser-induced pyrolysis, sonochemical process, and spray pyrolysis. Particle formation mechanisms are poorly understood for many of these

methods, and the final particle size and distribution are not well controlled. However, radiation-induced preparation of metal nanoparticles has various advantages compared with the other conventional methods because of its simplicity, easy process control, temperature independence, homogeneous reduction and nucleation of the nanoparticles, and absence of reducing agents or undesired oxidation byproduct impurities, thus it is harmless and environmentally benign. Also, this method provides metal nanoparticles in a fully reduced, highly pure, and highly stable state. The radiation-induced method of metal nanoparticle preparation is of growing interest. It has shown tremendous potential in morphological control and particle size distribution by adjusting parameters such as absorbed dose, dose rate, metal precursor concentration, and stabilizing agents. Moreover, the radiation method can be used for fast production of large quantities of materials in nanoscale size and structure controllable, which makes them applicable on an industrial scale (Clifford *et al.*, 2016; Bekhit *et al.*, 2020).

The chemical environments created by γ-radiolysis are ideal for producing chemically pure nanoparticles. Gamma-radiation decomposes water molecules into several species, including some very powerful reducing ($\cdot e^-_{aq}$, $\cdot H$) and oxidizing species ($\cdot OH$, $H_2O_2$), which drive the solution redox reactions that produce the nanoparticles. These redox-active species consist only of H and O atoms. The reactive products (such as $\cdot OH$ and $\cdot e^-_{aq}$) recombine to reform water upon the termination of irradiation and hence leave no unwanted chemical wastes (Flores-Rojas *et al.*, 2020; Yang *et al.*, 2020; Sen *et al.*, 2020).

This study has used gamma radiation to synthesize inorganic visible light-induced catalyst nanoparticles for the degradation of MB. The application of ionizing radiation, *i.e.*, gamma radiation, is becoming a promising clean technology to process materials. Using gamma radiation with nanomaterials offers several advantages, including continuous operation, minimum time requirement, less atmospheric pollution, curing at ambient temperatures, increased design flexibility through process control, etc. (Chowdhury *et al.,* 2006; Shubhra and Alam, 2011). This technique will effectively synthesize uniform and minimum-size nanoparticles for photocatalytic activity.

## Materials and Methods

### Materials

The ingredients used to produce nanostructured $Co_3O_4$ were all of the best possible analytical grade. Cobalt (II) nitrate hexahydrate $[Co(NO_3)_2 \cdot 6H_2O]$ as $Co^{2+}$ source (Research Lab Fine Chem Indusrties, Mumbai, India), distilled water, isopropyl alcohol $[(CH_3)_2CHOH]$ (Research Lab Fine Chem Industries, Mumbai, India) anhydrous sodium hydroxide [NaOH] (Sigma-Aldrich, Germany) polyvinyl alcohol [PVA] (Merck) and ammonium buffers (Sigma -Aldrich).
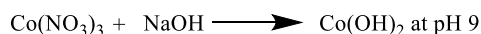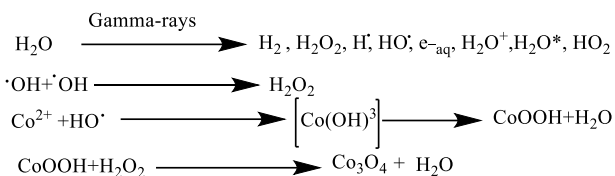
### Methods

#### Synthesis of Co(OH)₃

An experimental setup was established before subjecting the prepared sols to γ-irradiation. CoO(OH) sols were generated by using $Co(NO_3)_2 \cdot 6H_2O$, resulting in the formation of a $Co(OH)_2$ precipitate. Anhydrous sodium hydroxide was added into an aqueous solution of $Co(NO_3)_2 \cdot 6H_2O$ with a concentration of 0.04 mol/L, while continuously stirring with a magnetic stirrer until the pH of the suspension reached approximately 9. Ammonium buffers were chosen to prevent the irreversible precipitation of unwanted cobalt salts, which can occur in buffers containing carbonates or phosphates. The resulting sols were reddish, indicating the presence of cobaltous hydroxide $[Co(OH)_2]$ at a pH of approximately 9.

To facilitate the formation of $Co(OH)_3$, a concentrated solution of anhydrous NaOH was gradually added dropwise to the solutions while continuously stirring until a brown solution was obtained at a pH of about 12. This pH range promotes the formation of $Co(OH)_3$. The precipitate was then separated from the mother solution through repeated filtration and centrifugation. Subsequently, it was washed with ethyl alcohol to remove soluble salts, chloride ions, and cobalt oxyhydroxide. After 2 hours, CoO(OH) was obtained from $Co(OH)_3$ in the presence of air. The schematic chemical reaction is represented as:

### Preparation of CoO(OH) before γ-irradiation

$$Co(NO_3)_3 + NaOH \longrightarrow Co(OH)_2 \text{ at pH } 9$$
$$Co(NO_3)_3 + NaOH \longrightarrow Co(OH)_3 \text{ at pH } 12$$
$$Co(OH)_3 \longrightarrow CoO(OH) \text{ after two hour in air}$$

### Radiolytic Production of CoO₃O₄

$$H_2O \xrightarrow{\text{Gamma-rays}} H_2, H_2O_2, H^{\cdot}, HO^{\cdot}, e^-_{aq}, H_2O^+, H_2O^*, HO_2$$
$$\cdot OH + \cdot OH \longrightarrow H_2O_2$$
$$Co^{2+} + HO^{\cdot} \longrightarrow [Co(OH)^3] \longrightarrow CoOOH + H_2O$$
$$CoOOH + H_2O_2 \longrightarrow Co_3O_4 + H_2O$$

The resulting precipitates were dried in a vacuum oven at 60 °C for 4 hours and subjected to X-ray diffraction (XRD) analysis to determine their characteristics, while their morphology was observed using a scanning electron microscope (SEM).

### Gamma (γ)-irradiation Synthesis of Co₃O₄ Nanoparticles

On the contrary, when the CoO(OH) sols were formed at a pH of approximately 12, were mixed with a sodium carbonate solution (0.01 mol/L) to maintain a constant pH value of around 12. To enhance the production yield of nanoparticles, a solution of isopropyl alcohol (3.0 mol/L) was initially added to scavenge the oxidative radicals OH* generated during the radiolysis of water under gamma irradiation. This step aimed to prevent particle aggregation and promote nanoparticle formation. Additionally, a polyvinyl alcohol (PVA) organic surfactant (1% w/w) was introduced into the solution to inhibit the close contact and further aggregation of small particles.

The prepared sols were exposed to radiation using a $^{60}Co$ γ-ray source. The absorbed dose during irradiation was 30 kGy, with a dose rate of approximately 10 kGy/h. Following γ-irradiation, black precipitates were obtained, which were subsequently separated by washing with distilled water and absolute alcohol to remove any by-products. Finally, the precipitates were dried in a vacuum oven at 60 °C for 4 hours. The resulting black precipitate consisted of pure $Co_3O_4$, which was further annealed at 400 °C for 3 hours. The obtained product was collected and subjected to various characterization techniques for analysis.
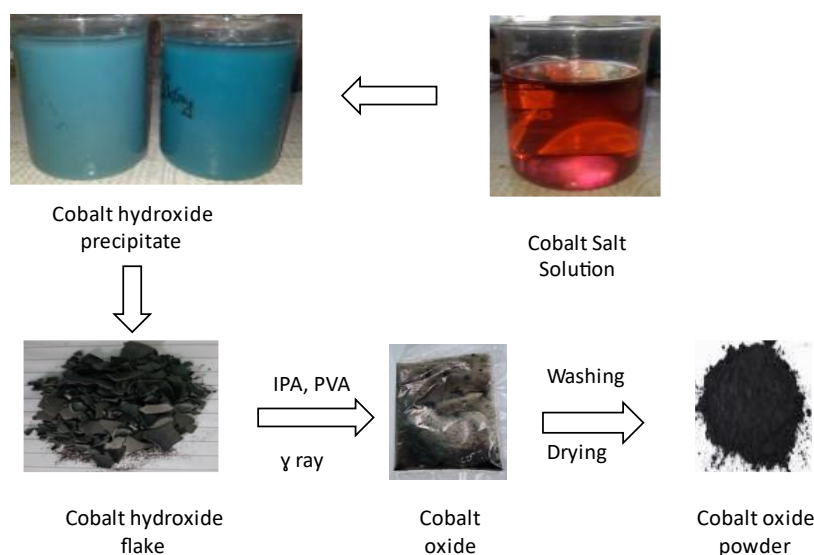
**Figure 1.** Schematic representation of the methodology for the synthesis of $CoO_3O_4$.

*Photodegradation of Textile Dyes*

The photocatalytic properties of $Co_3O_4$ nanoparticles were evaluated by performing a degradation experiment using methylene blue (MB) under a calibrated solar simulator with a 500W Xenon arc lamp and a lighting intensity of $100mW/cm^2$ at 1.5G. To initiate the experiment, a glass beaker containing 500 mL of double distilled water was utilized to thoroughly mix an aqueous solution of MB ($1\times10^{-5}$ M) with 0.031 g of $Co_3O_4$ catalyst. Subsequently, the resulting suspension was exposed to solar light without any agitation. At regular intervals of 45 min., samples of the degraded dye were extracted and subsequently centrifuged. The extent of photocatalytic degradation was assessed by measuring the absorbance of the samples using a UV spectrophotometer.

*Characterization*

*Fourier Transform Infrared (FT-IR) Spectroscopy*

The FT-IR spectroscopic analysis was carried out using the standard attenuated total reflection (ATR) technique using the PerkinElmer FT-IR spectrometer (Model: L1600300 Spectrum TWOLITA).

*X-ray Diffraction (XRD)*

The microstructure was assessed by using the X-ray diffractogram. X-ray diffraction (XRD) data were collected using a Rigaku Mini Flex II, Japan, operated at 30 kV, at 15 mA and equipped with computer software to analyze the data. The specimens were step-wise scanned over the operational range of scattering angle ($2\theta$) from 3 to 80°, with a step of 0.02°, using $CuK_\alpha$ radiation of wavelength $\lambda=1.541$ Å. The data were recorded in terms of the diffracted X-ray intensities (I) versus $2\theta$. The crystallographic lattice spacing ($d$) was calculated by following Bragg's equation (*Suh et al.*, 2000).

$$\lambda = 2dSin\theta \tag{1}$$

The average size of the crystallites, D, was determined with the full width at half-maximum (FWHM) of XRD peak by using the following Scherer's equation (Inagaki *et al.*, 2010):

$$D = \frac{0.9\lambda}{\delta Cos\theta} \tag{2}$$

Where, $\delta$ is the FWHM (in radians), and $\theta$ is the diffraction angle. The $\delta$ value was determined by curve fitting after subtracting the amorphous background. Using an appropriate program, the Gaussian curve was fitted at the top of the peak to determine $\delta$ and the position.

*Scanning Electron Microscopy*

The surface morphology of specimens was studied by the scanning electron microscope or SEM (TESCAN, VEGA3, Czech Republic). Samples were mounted on aluminium stubs with carbon tape analyzing them by SEM.

*Thermogravimetric Analysis (TGA)*

Thermogravimetric analysis (TGA) was performed by a TGA Q500 V6.4, Germany, in a platinum crucible, ramping from room temperature to 800 ºC at 10 ºC/min in the nitrogen atmosphere. The decomposition temperature was evaluated at different weight loss percentages, and residue content was determined at the final heating stage. Finally, the thermal stabilities of the material were determined using weight loss by this ramping method.

*UV-visible Spectroscopy*

The optical absorption spectra of the specimen solutions were recorded before and after exposure to visible light using a UV-visible spectrophotometer model (Perkin-Elmer Lambda 35). The baseline measurement was conducted automatically by the spectrophotometer with water as a reference.
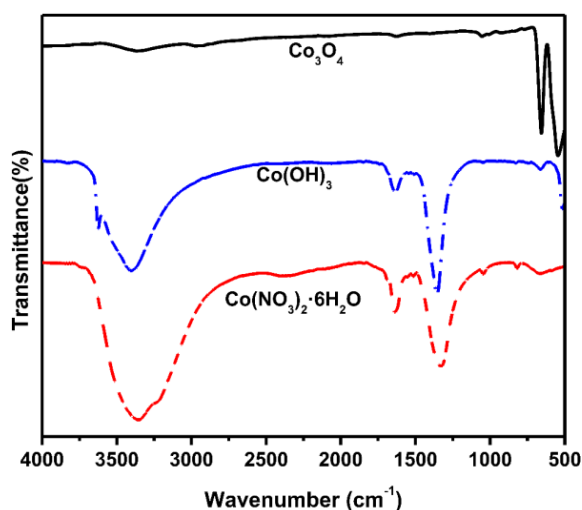
**Results and Discussion**

*FT-IR Analysis*



**Figure 2.** FT-IR spectra of raw $Co(NO_3)_2 \cdot 6H_2O$, $Co(OH)_3$ and $Co_3O_4$.

Figure 2 exhibits the characteristic FT-IR spectra of raw cobalt salt $[Co(NO_3)_2.6H_2O]$, cobalt hydroxide $[Co(OH)_3]$, and cobalt oxide $[Co_3O_4]$ molecules. The FTIR spectrum of $Co(NO_3)_2.6H_2O$ exhibits several characteristic peaks; the broad and strong peak at 3352 $cm^{-1}$ corresponds to the stretching vibration of O-H bonds in water molecules. A sharp peak at 1638 $cm^{-1}$ indicates the presence of the nitrate $(NO_3^-)$ ion with a symmetric stretching vibration of the nitrate group. A medium intensity peak at 1324 $cm^{-1}$ corresponds to the asymmetric stretching vibration of the nitrate group. The strong peak at 1039 $cm^{-1}$ suggests the presence of nitrate ions $(NO_3^-)$ with a characteristic bending vibration. A weak peak at 819 $cm^{-1}$ indicates the presence of Co-O stretching. A weak peak at 675 $cm^{-1}$ corresponds to Co-N stretching vibrations (Mashao *et al.*, 2019). In the case of $Co(OH)_3$ the broad and strong peak at 3403 $cm^{-1}$ corresponds to the stretching vibration of O-H bonds in hydroxide groups. The sharp peak at 1642 $cm^{-1}$ indicates the presence of the hydroxide ion with a symmetric stretching vibration of the $OH^-$ group (Su *et al.*, 2009). The medium intensity peak at 1356 $cm^{-1}$ corresponds to the asymmetric stretching vibration of the OH group. The medium intensity peak at 661 $cm^{-1}$ suggests the presence of Co-O stretching vibrations. The weak peak at 524 $cm^{-1}$ indicates the presence of Co-OH bending vibrations (Xie *et al.*, 2010).

The spectrum of $Co_3O_4$ exhibits a strong intensity peak at 661 $cm^{-1}$ corresponding to Co-O stretching vibrations. The medium intensity peak at 545 $cm^{-1}$ indicates the presence of Co-O stretching vibrations (Guan *et al.*, 2003).Therefore, the FT-IR analysis revealed that the 30 kGy irradiation dose is adequate for completely decomposing the precursor into the $Co_3O_4$ phase.

*XRD Analysis*

Figure 3 represents the X-ray diffractogram of $Co_3O_4$. The planes of $Co_3O_4$ (311), (002), (422) and (220) corresponded to the diffraction angles 2θ = (36.87°, 44.77°, 59.37° and 65.23°) (Prabaharan *et al*, 2017; Teng *et al,* 2008). Based on the given X-ray diffraction data for $Co_3O_4$, we can perform various analyses to obtain information about the lattice spacing, crystal size, and grain boundary.

Table 1 shows the calculated lattice spacing ($d$), and crystallite size ($D$), for $Co_3O_4$ nanoparticles.

**Table 1.** Lattice Parameters for Gamma-irradiated $Co_3O_4$ Nanoparticles

| Sample Name | 2θ (°) | Lattice spacing ($d$) Å | crystallite size ($D$) nm |
|---|---|---|---|
| | 36.87223 | 2.4912 | 36.1 |
| $Co_3O_4$ | 44.88804 | 2.0541 | 15.7 |
| | 59.37972 | 1.5515 | 27.4 |
| | 65.23258 | 1.4323 | 26.6 |

The 2θ values of the diffraction peaks are related to the lattice spacing calculated for each peak through Bragg's law represented by the equation (1):

Therefore, we can see that the lattice spacing decreases as the diffraction angle increases, which is consistent with the known crystal structure of CoO (rock salt structure).
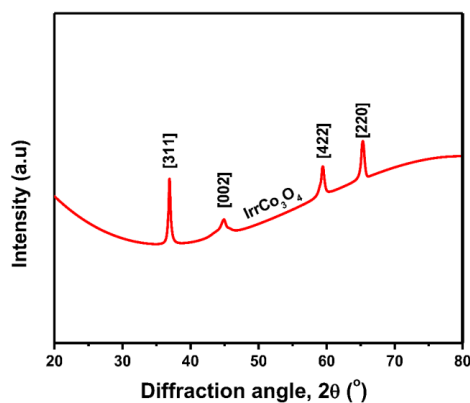


**Figure 3.** X-ray diffractogram of $Co_3O_4$.

The FWHM values of the diffraction peaks are related to the crystal size calculated for each peak through the Scherrer equation (2):
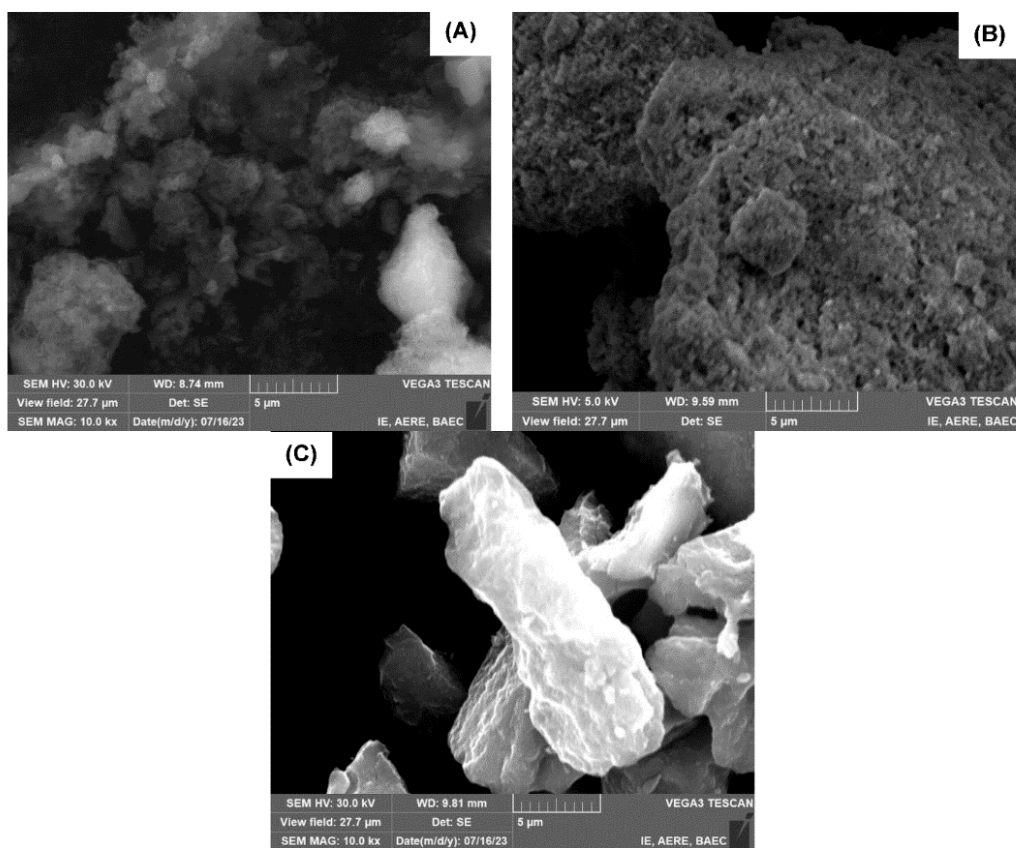


**Figure 4.** Scanning electron micrographs of A) raw cobalt nitrate salt, B) synthesized $Co(OH)_3$, and C) radiation-synthesized $Co_3O_4$.

Therefore, it is evident that the crystallite size of $Co_3O_4$ is in the nanometer range.

*Grain Boundary Analysis*

The broadening of the diffraction peaks in the FWHM values can also provide information about the grain boundary. The broadening is caused by the presence of small crystallites or defects in the crystal structure, which cause scattering of X-rays at slightly different angles. In summary, the X-ray diffraction data for $Co_3O_4$ shows that the crystal size is in the nanometer range, the lattice spacing decreases with increasing diffraction angle, and the degree of broadening in the diffraction peaks can provide information about the grain boundary.

*Surface Morphology*

Figure 4 demonstrates the surface morphology of A) Raw Cobalt Nitrate Salt, B) Chemical Synthesized precursor $Co(OH)_3$, and C) Radiation Synthesized $Co_3O_4$.
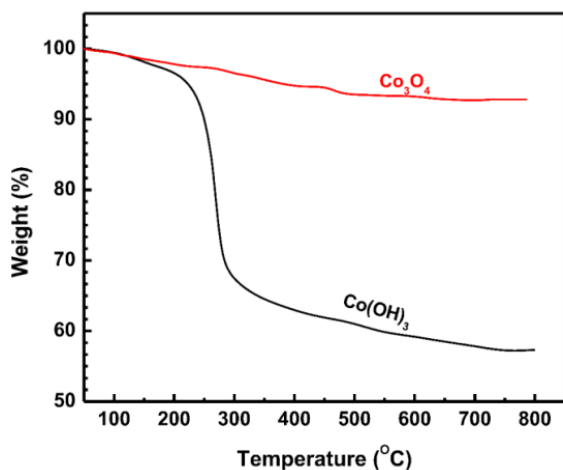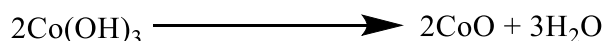
*Thermogravimetric Analysis (TGA)*



**Figure 5**. TGA thermograms of $Co(OH)_3$.
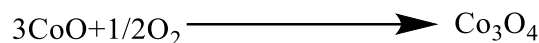
This fact can be explained as the radiolysis of $Co(OH)_3$ precursors can happen at elevated conditions, and aggregation of the nanoparticles occurs. The crystalline $Co_3O_4$ particles were observed as crystals in the micrographs of $Co_3O_4$. Large and agglomerated particles have been synthesized because the nucleation rate is lower than the particle growth rate. As a result, the produced cobalt sample is non-uniform and completely agglomerated (Allaedini and Muhammad, 2013).

Figure 5 demonstrates the decomposition pattern of $Co(OH)_3$ and radiation-synthesized $Co_3O_4$ nanoparticles in the thermogravimetric analysis curves under a nitrogen atmosphere. The thermogram of $Co(OH)_3$ typically involves moisture and adsorbed water removal, decomposition of $Co(OH)_3$ to CoO, and formation of $Co_3O_4$. At lower temperatures (below 210 °C), the TGA curve shows an initial mass loss of around 5% due to the evaporation of moisture and adsorbed water (Sinkó *et al.*, 2011). This step is usually characterized by a gradual decrease in weight. As the temperature increases (typically between 210 °C and 318 °C), $Co(OH)_3$ begins to decompose into cobalt oxide (CoO) and water ($H_2O$) (Zhang *et al.*, 2012). This step is noticed by a more significant weight loss on the TGA curve, corresponding to the release of water vapor. The reaction can be represented as:

$$2Co(OH)_3 \longrightarrow 2CoO + 3H_2O$$

At higher temperatures (above 318 °C), CoO can further oxidize to form $Co_3O_4$. In a nitrogen atmosphere, this step might be limited due to the lack of oxygen. However, residual oxygen or slight impurities in the nitrogen stream can facilitate this transformation (Zhang *et al.*, 2012). The reaction can be represented as:

$$3CoO + 1/2O_2 \longrightarrow Co_3O_4$$

Therefore, $Co(OH)_3$ showed a multi-step weight loss pattern corresponding to the dehydration of $Co(OH)_3$, followed by its decomposition to CoO, and potentially the formation of $Co_3O_4$.
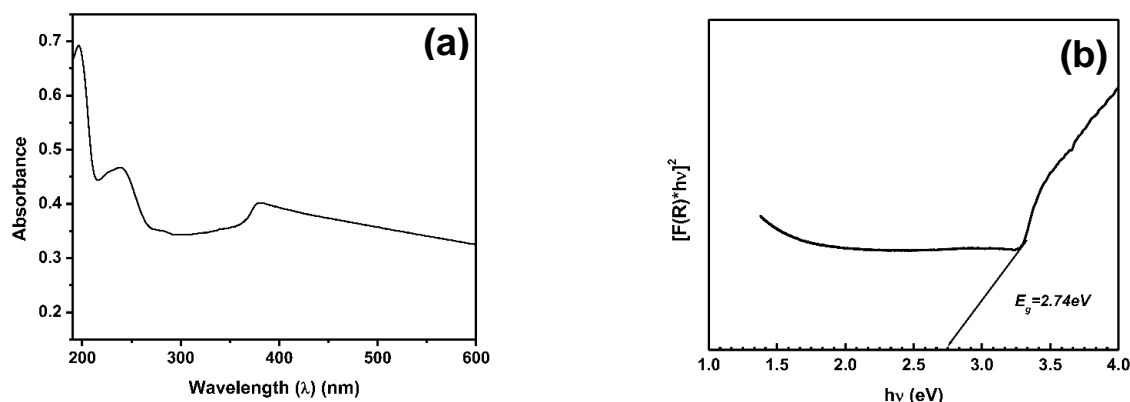
**Figure 6.** UV-vis spectrum of radiation synthesized $Co_3O_4$ nanoparticles (a) and optical bandgap of $Co_3O_4$ nanoparticles (b).

*UV-visible Spectrum and Direct Band Gap Energy Calculation of Radiation Synthesized $Co_3O_4$ Nanoparticles*

The decomposition pattern of $Co_3O_4$ nanoparticles in the TGA thermogram typically involves a distinct thermal behavior due to the stability of $Co_3O_4$. At lower temperatures (up to around 140 °C), the TGA curve exhibited a minor initial mass loss due to the evaporation of surface moisture and adsorbed water on the nanoparticles. This is typically a small and gradual decrease in weight. From around 140 °C to 800 °C, $Co_3O_4$ is generally stable, and no significant weight loss is observed. The TGA curve appeared relatively flat in this temperature range, indicating the thermal stability of $Co_3O_4$ under an inert atmosphere like nitrogen.

The UV-visible spectrum of radiation synthesized $Co_3O_4$ was recorded in an aqueous solution, and the direct band gap energy was calculated using the following Kubelka-Munk (K-M) function based on the optical absorption equation (Landi *et al.*, 2022; Hossain *et al.*, 2018):

$$[F(R) \times h\vartheta]^{(1/n)} = A(h\vartheta - E_g) \qquad (3)$$

where $n$ is a constant that defines the type of transition, A is the proportionality constant, $h\nu$ is the photon energy, F(R) is the absorption coefficient, and $E_g$ is the optical band gap value.

The radiations-synthesized $Co_3O_4$ nanoparticles exhibit a direct type optical band gap, as evidenced by the presence of a straight line in the spectra. The factor n, whose value depends on the transition modes, characterizes the optical transition process. The direct allowed, indirect allowed, direct forbidden, and indirect forbidden modes correspond to n values of 1/2, 2, 3/2, and 3, respectively (Sen *et al.*, 2022).

As shown in Figure 6(b), the direct band gap $E_g$) of the $Co_3O_4$ nanoparticles can be calculated using a plot of $[F(R) \times h\vartheta]^2$ as a function of $h\vartheta$.. The value of $E_g$ for $Co_3O_4$ nanoparticles is estimated by the intercept of $[F(R) \times h\vartheta]^2$ on the energy axis (x-axis). The $E_g$ value is 2.74 eV, which falls within the visible light band gap range of 1.6 eV to 3.2 eV.

*Evaluation of Catalytic Effect on Textile Dye Degradation*

The research investigated the effectiveness of $Co_3O_4$ nanoparticles synthesized through radiation for degrading MB, a textile dye. The photocatalytic activity of the nanoparticles was examined by exposing them to visible light at room temperature.
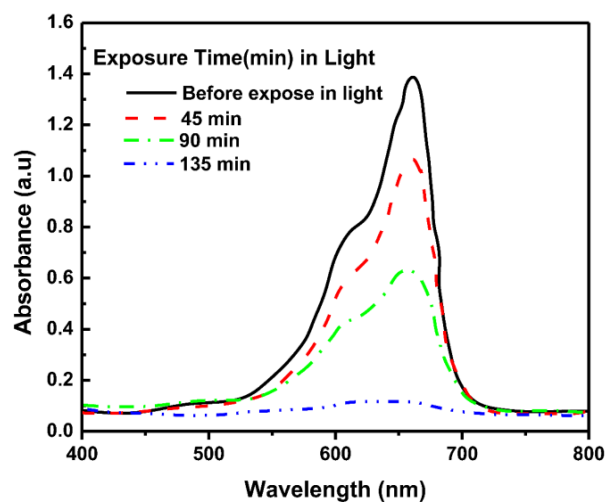


**Figure 7.** Evolution of UV-vis absorption spectra of textile dye (methylene blue) in the presence of $Co_3O_4$ nanoparticles exposed to visible light at different times.

The UV–vis spectra analysis of MB aqueous solution with the presence of $Co_3O_4$ nanoparticles photocatalyst under visible light exposure ($\lambda>420$ nm) was conducted over different time intervals, as illustrated in the accompanying Figure 7. MB dye exhibits a characteristic absorption peak around 664 nm, which diminishes noticeably as the exposure time increases. This decrease is attributed to the continuous degradation of MB molecules through photocatalytic processes. After an exposure of 135 minutes, the absorbance of the MB solution falls below 0.11, indicating substantial degradation of the dye molecules.
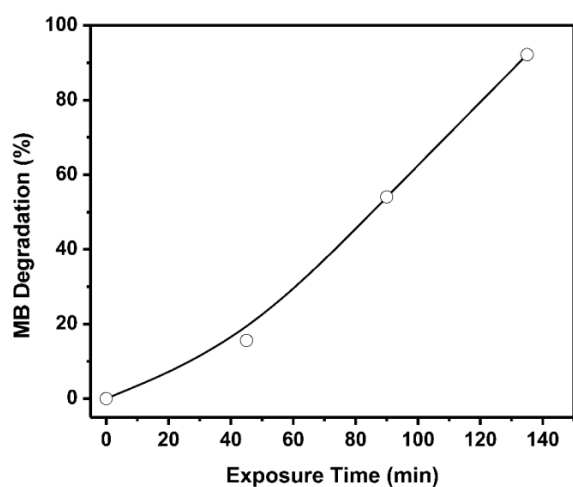


**Figure 8.** Degradation of methylene blue (MB) dye by radiation-synthesized $Co_3O_4$ nanoparticles exposed to visible light at 45, 90, and 135 minutes.

The degradation percentage of methylene blue (MB) concerning exposure time is represented in Figure 8. The degradation percentages increased from 15.6% to 92.2% as the exposure time was extended from 45 minutes to 135 minutes under visible light. This demonstrates that radiation-synthesized $Co_3O_4$ nanoparticles exhibit a significant photocatalytic effect for the degradation of MB dye.

## Conclusions

This study demonstrates that the synthesis of $Co_3O_4$ nanoparticles from $Co(OH)_3$ precursor using a $^{60}Co$ gamma radiation source is a viable method. The synthesized $Co_3O_4$ nanoparticles exhibit properties comparable to those produced by conventional methods, as confirmed by various characterization techniques. The radiation-synthesized $Co_3O_4$ nanoparticles displayed a direct optical band gap of 2.74 eV, which falls within the visible light range, making them suitable for visible light applications. Furthermore, the nanoparticles exhibited significant photocatalytic activity under visible light, effectively degrading MB dye. The degradation percentage of MB increased substantially with prolonged exposure, demonstrating the potential of these nanoparticles for practical photocatalytic applications in environmental remediation. The findings of this study suggest that radiation-synthesized $Co_3O_4$ nanoparticles could be effectively used for the degradation of organic pollutants under visible light, offering a promising approach for environmental cleanup. Future research could explore the optimization of synthesis parameters and the potential application of these nanoparticles in different photocatalytic processes, further enhancing their utility and effectiveness in various environmental and industrial applications.

## Acknowledgements

## Declaration

The authors declare that the research findings reported in this manuscript do not have any conflicting interests.

## Authors' Contribution

MSM, MRI and AKMMA contributed to the conceptualization of the research, designed the experiments, conducted experimental work, prepared samples, collected and analyzed data, drafted the manuscript, and supervised the research. MAM and MMR supported sample characterization and analysis. MFM facilitated sample irradiation using a cobalt-60 gamma source.

## References

Allaedini G and Muhammad A 2013. Study of influential factors in synthesis and characterization of cobalt oxide nanoparticles. *Journal of Nanostructure in Chemistry* **3**: 1−16.

Bekhit M, Abu el-naga MN, Sokary R, Fahim RA and El-Sawy NM 2020. Radiation-induced synthesis of tween 80 stabilized silver nanoparticles for antibacterial applications. *Journal of Environmental Science and Health, Part A* **55**(10): 1210−1217.

Chmielewski AG, Michalik J, Buczkowski M and Chmielewska DK 2005. Ionising radiation in nanotechnology. *Nuclear Instruments and Methods in Physics Research Section B: Beam Interactions with Materials and Atoms* **236**(1−4): 329−332.

Chmielewski AG, Chmielewska DK, Michalik J and Sampa MH 2007. Prospects and challenges in application of gamma, electron and ion beams in processing of nanomaterials. *Nuclear Instruments and Methods in Physics Research Section B: Beam Interactions with Materials and Atoms* **265**(1): 339−346.

Chowdhury MNK, Alam AKMM, Dafader NC, Haque ME, Akhtar F, Ahmed M U and Begum R 2006. Radiation processed hydrogel of poly (vinyl alcohol) with biodegradable polysaccharides. *Bio-medical Materials and Engineering* **16**(3): 223−228.

Clifford DM, Castano CE and Rojas JV 2017. Supported transition metal nanomaterials: nanocomposites synthesized by ionizing radiation. *Radiation Physics and Chemistry* **132**: 52−64.

Chatterjee D and Dasgupto S 2005. Visible light induced photocatalytic degradation of organic pollutants. *Journal of Photochemistry and Photobiology C: Photochemistry Reviews* **6**:186–205.

Flores-Rojas GG, López-Saucedo F and Bucio E 2020. Gamma-irradiation applied in the synthesis of metallic and organic nanoparticles: A short review. *Radiation Physics and Chemistry* **169**: 107962.

Guan H, Shao C, Wen S, Chen B, Gong J Yang and X 2003. A novel method for preparing $Co_3O_4$ nanofibers by using electrospun PVA/cobalt acetate composite fibers as precursor. *Materials Chemistry and Physics* **82**(3): 1002−1006.

Hossain MK, Mortuza AA, Sen SK, Basher MK, Ashraf MW, Tayyaba S, Mia MN and Uddin MJ 2018. A comparative study on the influence of pure anatase and Degussa-P25 $TiO_2$ nanomaterials on the structural and optical properties of dye sensitized solar cell (DSSC) photoanode. *Optik.* **171**: 507516.

Landi Jr S, Segundo IR, Freitas E, Vasilevskiy M, Carneiro J and Tavares CJ 2022. Use and misuse of the Kubelka-Munk function to obtain the band gap energy from diffuse reflectance measurements. *Solid State Communications* **341**: 114573.

Mashao G, Modibane KD, Mdluli SB, Iwuoha EI, Hato MJ, Makgopa K and Molapo KM 2019. Polyaniline-cobalt benzimidazolate zeolitic metal-organic framework composite material for electrochemical hydrogen gas sensing. *Electrocatalysis* **10**: 406−419.

Prabaharan DD, Sadaiyandi K, Mahendran M and Sagadevan S 2017. Precipitation method and characterization of cobalt oxide nanoparticles. *Applied Physics A* **123**: 1−6.

Sen SK, Manir MS, Nur S, Hossain N, Islam MJ, Alam AKMM and Hakim MA 2020. Estimation of hydrothermally synthesized Iron incorporated 2D-sheet-like α-$MoO_3$ microstructural and optical parameters treated by annealing temperature. *Materials Research Express* **7**(9): 095005.

Sen SK, Munshi MR, Kumar A, Mortuza AA, Manir MS, Islam MA, Hossain MN and Hossain MK 2022. Structural, optical, magnetic, and enhanced antibacterial properties of hydrothermally synthesized Sm-incorporating α-$MoO_3$ 2D-layered nanoplates. *RSC Advances* **12**(53): 34584−34600.

Shubhra QT and Alam AKMM 2011. Effect of gamma radiation on the m echanical properties of natural silk fiber and synthetic E-glass fiber reinforced polypropylene composites: A comparative study. *Radiation Physics and Chemistry* **80**(11): 1228−1232.

Sinkó K, Szabó G and Zrínyi M 2011. Liquid-phase synthesis of cobalt oxide nanoparticles. *Journal of Nanoscience and Nanotechnology* **11**(5): 4127–4135.

Song C, Wang Z, Yin Z, Xiao D and Ma D 2022. Principles and applications of photothermal catalysis. *Chem Catalysis* **2**(1): 52−83.

Su LH, Zhang XG, Mi CH, Gao B and Liu Y 2009. Improvement of the capacitive performances for Co−Al layered double hydroxide by adding hexacyanoferrate into the electrolyte. *Physical Chemistry Chemical Physics* **11**(13): 2195−2202.

Suh DJ, Lim YT and Park OO 2000. The property and formation mechanism of unsaturated polyester–layered silicate nanocomposite depending on the fabrication methods. *Polymer* **41**: 8557–8563.

Inagaki T, Siesler HW, Mitsui K and Tsuchikawa S 2010. Difference of the crystal structure of cellulose in wood after hydrothermal and aging degradation: a NIR Spectroscopy and XRD Study. *Biomacromol.* **11**: 2300–2305.

Teng F, Xu T, Zheng Y, Liang S, Gochoo B, Gu X, Zong R, Yao W and Zhu Y 2008. Formation of hollow NiO single crystals and Ag/NiO flowers. *Materials Research Bulletin* **43**(12): 3562–3569.

Xie X, Shang P, Liu Z, Lv Y, Li Y and Shen W 2010. Synthesis of nanorod-shaped cobalt hydroxycarbonate and oxide with the mediation of ethylene glycol. *The Journal of Physical Chemistry C* **114**(5): 2116–2123.

Yang Y, Johansson M, Wiorek A, Tarakina NV, Sayed F, Mathieu R, Jonsson M and Soroka IL 2021. Gamma-radiation induced synthesis of freestanding nickel nanoparticles. *Dalton Transactions* **50**(1): 376–383.

Zhang F, Yuan C, Lu X, Zhang L, Che Q and Zhang X 2012. Facile growth of mesoporous $Co_3O_4$ nanowire arrays on Ni foam for high performance electrochemical capacitors. *Journal of Power Sources* **203**: 250–256.